Application of numerical continuation to bifurcation analysis of Rijke tube

Priya Subramanian[*1], Sathesh Mariappan[2], R. I. Sujith[3] & Pankaj Wahi[4]

[1], [2], [3] Department of Aerospace Engineering, Indian Institute of Technology Madras
Chennai-600036, India
[4] Department of Mechanical Engineering, Indian Institute of Technology Kanpur
Kanpur-201086, India
[*] Corresponding author: iitm.priya@gmail.com

Bifurcation analysis of the dynamical behavior of a horizontal Rijke tube model is performed in this paper. Numerical continuation method is used to obtain the bifurcation plots, including the amplitude of the unstable limit cycles. Linear and nonlinear stability boundaries are obtained for the simultaneous variation of two parameters of the system. Bifurcation plots for the variation of nondimensional heater power, damping coefficient and the heater location are obtained which display subcritical Hopf bifurcation. Regions of global stability, global instability and bistability are characterized. The validity of the small time lag assumption in the calculation of the linear stability boundary has been shown to fail at typical values of time lags of the system. Accurate calculation of the linear stability boundary in systems with explicit time delay models, must therefore, not assume a small time lag assumption.

1 Introduction

Combustion instability is a plaguing problem in the development of combustors for rockets and gas turbines used in jet engines and power generation [17]. Fluctuations in heat release rate can both arise due to and act as a source of acoustic fluctuations, causing the coupled system to reach self-sustained large amplitude oscillations. Combustion instability is caused when the fluctuating heat release rate and the acoustic field form a positive feedback loop.

In linear stability analysis, when all the eigenvalues of the system are in the left half of the complex plane, the eigenmodes of the system have negative growth rates and therefore the system is linearly stable. If one or more of the eigenvalues lie on the right half of the complex plane, correspondingly the eigenmodes have positive growth rates and the system is linearly unstable. In a linearly unstable system, any infinitesimal initial perturbation grows exponentially and asymptotically reaches a limit cycle. A linearly stable system can also exhibit subcritical transition to instability and asymptotically reach a limit cycle for suitable initial conditions. This type of subcritical transition to instability from a finite amplitude initial condition is called triggering.

Triggering has been exhibited in solid rocket motors [23] and also in a Rijke tube [16]. Triggering can cause a system which is linearly stable to become unstable in the presence of a finite amplitude disturbance. Therefore in systems exhibiting subcritical transition to instability, it is important to determine the nonlinear stability boundaries and the limit cycle characteristics through nonlinear stability analysis.

We will perform nonlinear stability analysis of a thermoacoustic system by using a simple model for thermoacoustic oscillations in a horizontal Rijke tube [3] that displays the essential features. Rijke tube is an acoustic resonator tube, which consists of a heat source (in the present case, an

electrical heater), positioned at some axial location. A mean flow is maintained at a desired flow rate using a blower. A correlation between the heat release rate fluctuations at the heater location and the acoustic velocity fluctuations at the heater [10] is used to model the fluctuating heat release rate from the heater in the Rijke tube [3]. In the present paper, we use this model problem to understand the nonlinear dynamics in a Rijke tube. Approaches used to study instability in a Rijke tube are briefly reviewed below.

1.1 Thermoacoustic instability in a Rijke tube

Self sustained thermoacoustic oscillations are observed in the Rijke tube when the heater is positioned at certain axial locations of the tube and beyond some threshold power level. Linear models for the unsteady heat release rate due to the acoustic velocity fluctuations were used to calculate linearly unstable locations along the Rijke tube [4]. The stability thus predicted is the linear stability of the system; i.e. the stability of oscillations in the asymptotic time limit for small amplitude oscillations. Therefore this method cannot predict finite amplitude effects such as triggering instabilities and the limit cycle characteristics. Estimation of the amplitude of acoustic oscillations during limit cycle is important from the design point of view for gas turbines. For this, the nonlinearity in the heat release rate response of the heater has to be included [14] in the analysis. CFD based analysis was also used to study Rijke tube oscillations with the heat source being considered as a heated flat plate [9] or as flow over a cylinder [15].

In most of the cases, solving the governing equations to obtain the unsteady heat transfer from the heater is computationally expensive. For those cases, a lower order model is used to simulate the nonlinear response of the heater. A low order time lag model based on a correlation for the heat release rate given by Heckl [10] has been used to model the dynamics of the heater [3]. The Rijke tube model thus obtained still retains the diverse dynamical behavior of the thermoacoustic instability in a Rijke tube and exhibits nonlinear phenomena such as subcritical transition to instability and limit cycles. Bifurcation analysis of low dimensional models of systems has been studied using many techniques for aeroelastic problems [5] and for combustion instabilities in combustion chambers [2, 12]. This analysis can be used to identify the nature of the transition to instability and to characterize the finite amplitude oscillations produced. A brief review of the techniques used in bifurcation analysis is given below.

1.2 Bifurcation analysis techniques

The approach of obtaining bifurcation diagrams by systematic variation of parameter and tracking direct time integration was used by Moeck [18], Mariappan & Sujith [15]. This method is computationally expensive. Moreover, the basins of attraction obtained for the limit cycle and the steady state remain specific to the type of initial condition applied, making it not suited for systems which exhibit pulsed instability [2]. Many alternate approaches for bifurcation analysis are available such as cell mapping [11], higher order harmonic balancing [21] and numerical continuation [1, 2]. Of these methods, numerical continuation has lesser errors of approximation and is versatile in capturing all types of bifurcations.

Numerical continuation aims to solve a set of parameterized nonlinear equations iteratively given an initial guess for the state of the system. Solutions which satisfy the set of equations and which are additionally connected to the initial state, for a given smooth variation of one or more parameters are obtained by tracking the solution curve in the state space. Bifurcations are identified by including multiple test functions which change sign at the critical value of the parameter. This method has the advantage that once a stationary or periodic solution has been computed, the dependence of the solution on the variation of a parameter is obtained very efficiently as compared with the other methods described earlier. It can also be used to compute unstable limit cycles.

Numerical continuation has been used to obtain the amplitudes of longitudinal acoustic modes in a combustion chamber [12] and for the control of a thermoacoustic system [8]. Reduced order models for the combustion chambers have been solved by the framework of expanding the pressure and velocity fields in terms of modal or basis functions. Ananthakrishnan et al. [2], examined the

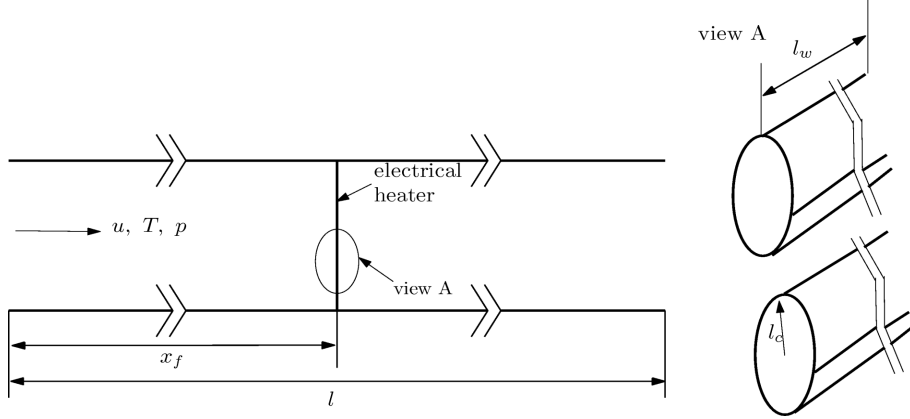Priya Subrmanian, Sathesh Mariappan, R. I. Sujith & Pankaj Wahi

Figure 1: Configuration of a horizontal Rijke tube with an electric heater as source.

issue of modal truncation and established the number of modes required to accurately capture the dynamics of the system.

However, in numerical continuation, the different types of equations encountered in models of physical systems require special attention during the analysis stage. As an example, numerical continuation methods used for models containing delay differential equations must be capable of handling time delay systems. The low order model used for the Rijke tube contains an explicit delay term. The numerical continuation package used in the present study is DDE-BIFTOOL [6,7] which is capable of handling delay differential equations. Determination of the bifurcation behavior of the Rijke tube including the unstable limit cycle is the objective of this paper.

The stability bounds of the state space with different parameters will also be obtained and the results validated with time marching solutions of the system. Significant system parameters to be varied are the non-dimensional heater power (K), location of heater (x_f), damping coefficient (c_1) and the time lag (τ). The rest of the paper is organized as follows. Section 2 describes the low order model for the Rijke tube and the formulation used in numerical continuation. Analysis of the results obtained from numerical continuation are presented in Section 3. The results of bifurcation analysis using numerical continuation for various parameters are summarized in Section 4. Section 5 lists the conclusions of the present work.

2 Model for Rijke tube

The Rijke tube model used in the present paper closely follows Balasubramanian & Sujith [3] and is for the geometry shown in Fig. 1. It is governed by the non-dimensional linearized acoustic momentum equation and acoustic energy equations as given below in Eqns. (1) and (2):

$$\gamma M \frac{\partial u'}{\partial t} + \frac{\partial p'}{\partial x} = 0 \tag{1}$$

$$\frac{\partial p'}{\partial t} + \gamma M \frac{\partial u'}{\partial x} + \zeta p' = (\gamma - 1)\dot{Q}'(t)\delta(x - x_f) \tag{2}$$

The response of the heat transfer from the wire filament to acoustic velocity fluctuations is quantified using the correlation given by Heckl [10]. The heat release rate fluctuations can then be rewritten in terms of the acoustic velocity fluctuations as given in Eqn. (3) and the damping ζ_j is obtained from a mode dependent damping given by Matveev [16] as shown in Eqn. (4).

$$\dot{Q}'(t) = \frac{2L_w(T_w - \bar{T})}{S\sqrt{3}} \sqrt{\pi \lambda C_V \bar{\rho} l_c} \left[\sqrt{\left| \frac{1}{3} + u'_f(t - \tau) \right|} - \sqrt{\frac{1}{3}} \right] \tag{3}$$

$$\zeta_j = \frac{1}{2\pi} \left(c_1 \frac{\omega_j}{\omega_1} + c_2 \sqrt{\frac{\omega_1}{\omega_j}} \right) \tag{4}$$

Here c_1 and c_2 are the damping coefficients which can be varied and which control the amount of mode dependent damping in the system. Further, l_c, L_w and T_w are the radius, length and temperature of the wire respectively, S is the cross sectional area, $\bar{T}$ is the mean temperature, λ is the thermal conductivity and C_v is the specific heat at constant volume of the medium within the duct.

The acoustic energy equation can be modified as given below by including the correlation for heat release rate fluctuations:

$$\frac{\partial p'}{\partial t} + \gamma M \frac{\partial u'}{\partial x} + \zeta p' = (\gamma - 1) \frac{2 L_w (T_w - \bar{T})}{S \sqrt{3}} \sqrt{\pi \lambda C_V \bar{\rho} l_c} \left[\sqrt{\left| \frac{1}{3} + u'_f(t - \tau) \right|} - \sqrt{\frac{1}{3}} \right] \delta(x - x_f) \tag{5}$$

The non-dimensional partial differential equations Eqn. (1) and Eqn. (5) can be reduced to a set of ordinary differential equations by expanding the acoustic variables in terms of basis functions using the Galerkin technique [24].

$$u' = \sum_{j=1}^{N} \cos(\omega_j x) U_j(t) \quad \text{and} \quad p' = \gamma M \sum_{j=1}^{N} \sin(\omega_j x) P_j(t) \tag{6}$$

$$\dot{U}_j + \omega_j P_j = 0 \tag{7}$$

$$\dot{P}_j + 2\zeta_j \omega_j P_j - \omega_j U_j = K \left[\sqrt{\left| \frac{1}{3} + u'_f(t - \tau) \right|} - \sqrt{\frac{1}{3}} \right] \sin(\omega_j x_f) \tag{8}$$

The resulting set of equations can be written as given in Eqns.(7) and (8) and are evolved in time. Here, $K = \left(4 L_w (T_w - \bar{T}) \sqrt{\pi \lambda C_V \bar{\rho} l_c} / S \sqrt{3} \gamma M \right)$ is the expression for the non-dimensional heater power (K). The equations can be simplified by expanding the term under the square root in Eqn. (8) under the assumptions of small acoustic velocity at the flame (u'_f) and small time lag (τ). The resulting equation, valid in the limit of small time lag, is written as given below in Eqn. (9).

$$\dot{P}_j + 2\zeta_j \omega_j P_j - \omega_j U_j = K \frac{\sqrt{3}}{2} \left[\sum_{i=1}^{N} \cos(\omega_i x) U_i(t) + \tau \sum_{i=1}^{N} \sin(\omega_i x) P_i(t) \right] \sin(\omega_j x_f) \tag{9}$$

3 Analysis

3.1 Steady-state equilibrium and linear stability analysis

As the initial step in performing the stability analysis for given parameter values, the steady state of the system for that set of parameters is calculated in DDE-biftool using the Newton's method. Next linear (local) stability of the obtained equilibrium is identified by examining the eigenvalues of the system linearized around the equilibrium. If all the eigenvalues lie on the left half plane, the equilibrium is linearly stable to small perturbations. When one or more eigenvalues of the linearized system lie on the right half plane, the system is said to be linearly unstable. Stability properties of the equilibrium is therefore changed when the real part of the most dominant eigenvalue crosses zero as some relevant parameter of the system is varied. The value of the parameter at which the real part of the most dominant eigenvalue is zero is called the bifurcation point.

The behavior of the system changes as this value of the parameter is crossed since the equilibrium solution looses stability. New steady states emerge from the bifurcation point depending on the type and nature of the bifurcation to be discussed in the next subsection. A bifurcation point is located in DDE-biftool by continuing the equilibrium solution branch with a variation in the relevant parameter and studying the spectrum of the first few dominant eigenvalues. Once a bifurcation point is located with respect to one parameter, the bifurcation point itself is continued
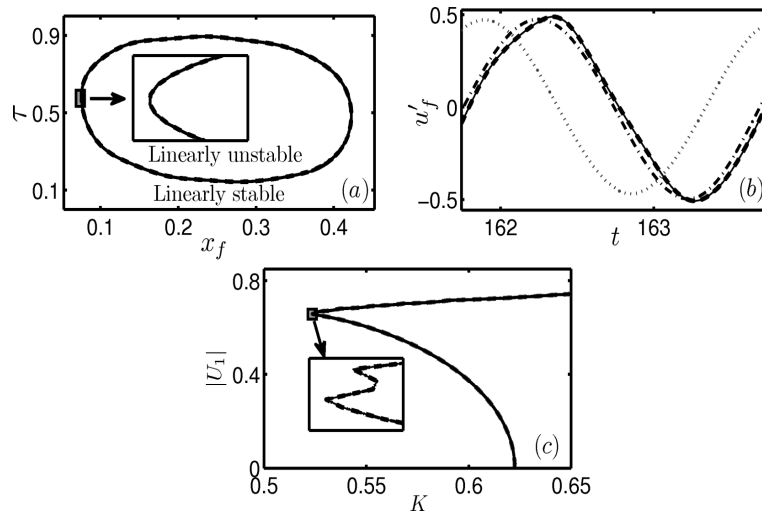
Figure 2: (a) Modal convergence of linear stability boundary between x_f and τ with $c_1 = 0.1$, $c_2 = 0.06$ and $K = 0.8$. (b) Comparison of limit cycle amplitude from time evolutions with different number of acoustic Galerkin modes (N) at $x_f = 0.3$. (c) Comparison of bifurcation plots for variation of non-dimensional heater power (K) with different number of acoustic Galerkin modes (N). In this figure, $\cdots\cdots$ N=1, $\cdot-\cdot-\cdot$ N=2, $---$ N=9 and $\underline{\hspace{0.5cm}}$ N=10. Grey areas are enlarged in inset figures to show convergence with increase in number of modes .

with a variation in a second relevant parameter of the system. The resulting branch of bifurcation points gives us the linear stability boundary which separates regions in the relevant parameter space with linearly stable and unstable equilibrium. This stability boundary is a high-dimensional hyper-surface in the space of all the free parameters of the system, but is most conveniently represented by a curve in several appropriate two-dimensional projections. A typical stability boundary for free variation of the heater location and the time lag of the system is shown in Fig. 2(a).

Figure 2(a) shows that for the chosen set of fixed parameter values for the damping and the heater power, the system is linearly unstable for a chosen range of heater locations (x_f) depending on the time lag τ of the system and vice versa. For very low and reasonably large values of τ such as $\tau < 0.15$ and $\tau > 0.85$ in Fig. 2(a), the system is linearly stable for any heater location. Only in the range $0.15 < \tau < 0.85$, the equilibrium solution can become unstable depending on the heater location. The stability boundary for different number of acoustic Galerkin modes from 1 mode to 10 modes show little variation for the case shown in Fig. 2(a). In the next section, we discuss limit cycles obtained using the nonlinear analysis and establish the convergence of the general solution of the system with 10 Galerkin modes.

3.2 Numerical simulation, limit cycles and nonlinear analysis

The bifurcation points at the linear stability boundary obtained in the previous section are associated with a pair of complex conjugate eigenvalues crossing the imaginary axis and accordingly, we have a Hopf bifurcation. Isolated periodic solutions called limit cycles emerge from the Hopf bifurcation point of the equilibrium solution. To check for the existence of such solutions and the convergence of the number of acoustic Galerkin modes, the time evolutions of the system with different number of acoustic modes for system parameters in the linearly unstable region are compared in Fig. 2(b). It can be seen from Fig. 2(b) that there is a limit cycle and also that the amplitude of the limit cycle shows very little variation with an increase in the number of acoustic Galerkin modes. The variation in the phase of the various solutions can be attributed to initial
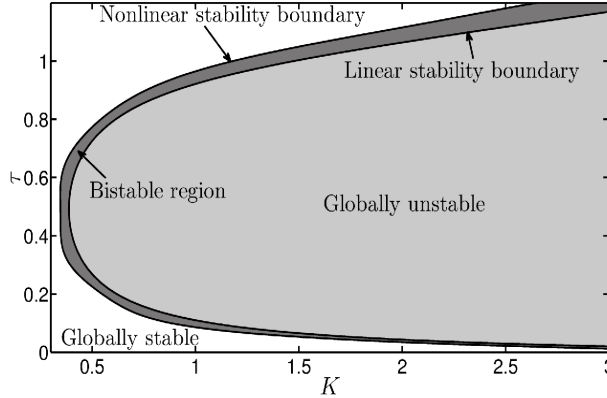
Figure 3: Region of bistability obtained for the bifurcation between non-dimensional heater power (K) and time lag (τ) with the other system parameters being $c_1 = 0.1$, $c_2 = 0.06$ and $x_f = 0.3$.

conditions. In fact, this difference is not visible in Fig. 2(c) wherein we have plotted the variation of the amplitudes of the first Galerkin mode with a variation in the heater power K. The measure used to quantify the asymptotic state ($t \to \infty$) of the system in Fig. 2(c) is the difference between the maximum and minimum value ($|U_1|$) of the non-dimensional first acoustic velocity mode which is twice the amplitude of the first velocity mode.

The amplitudes of the limit cycles in Fig. 2(c) are obtained using continuation of the limit cycles using DDE-biftool. In this figure, the equilibrium is stable for $K < 0.625$ and small-amplitude limit cycles originating from the Hopf bifurcation point also exist in this region. These limit cycles are unstable and the Hopf bifurcation is subcritical in nature. As the amplitude of these limit cycles increases in magnitude, these limit cycles stabilize through a 'turning point' or 'fold' bifurcation. The unstable branch of limit cycles turns around at $K = 0.523$ and in the region $0.523 < K < 0.625$, a stable equilibrium, an unstable small-amplitude limit cycle and a large-amplitude stable limit cycle coexist. This is the range of 'bistability' where the equilibrium is only locally stable and large amplitude disturbances grow to limit cycles. Below the fold bifurcation point, i.e., for $K < 0.523$ the equilibrium is globally stable to any perturbations.

For a model with 10 acoustic modes, an addition of more Galerkin modes changes the limit cycle amplitude of the acoustic velocity by less than 1.4%. Therefore, in all calculations considered henceforth, a model with 10 Galerkin modes is used to ensure convergence in the number of acoustic Galerkin modes for the linear and nonlinear stability analysis.

We noted in Fig. 2(c) that a subcritical Hopf bifurcation happens when the non-dimensional heater power is varied as the free parameter. This will also happen with variation in any other free parameter of the system as it is an inherent property of the nonlinearity present in the system. A qualitative argument to justify this claim is provided below. The nature of the bifurcation associated with a source term nonlinearity of the form $(1 \pm X)^\alpha$, where X is the state variable and α is a real number can be identified by expanding the nonlinearity in a series about small X and dropping higher order terms. A binomial expansion of the above expression results in the following equation.

$$1 \pm \alpha X \mp \frac{\alpha(\alpha - 1)}{2!} X^2 \pm \frac{\alpha(\alpha - 1)(\alpha - 2)}{3!} X^3 \mp \dots. \tag{10}$$

In the above expression, the signs of the first and the third order terms are seen to be same when $0 < |\alpha| < 1$ and $|\alpha| > 2$. The signs will be different when the value of α lies between $1 < |\alpha| < 2$. The relative signs of the first and the third order term dictates the nature of the bifurcation. Whenever these terms have the same sign, the bifurcation is subcritical while it is supercritical when these terms have different signs. This result has been obtained in the context
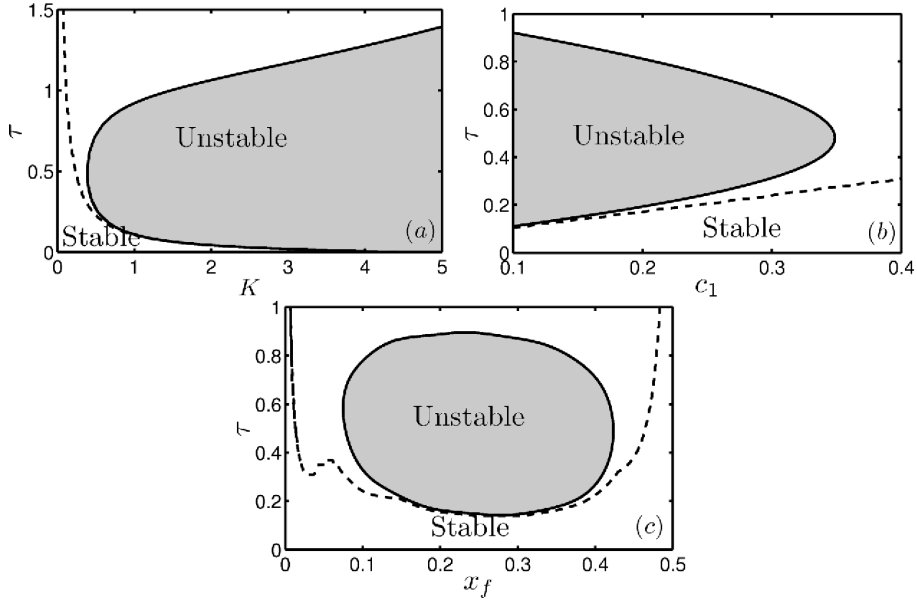
Figure 4: Comparison of stability boundary obtained with —— and without − − − the small time lag assumption between (a) non-dimensional heater power (K) and time lag (τ) with the other system parameters being $c_1 = 0.1$, $c_2 = 0.06$ and $x_f = 0.3$. (b) damping coefficient (c_1) and time lag (τ) for $c_2 = 0.06$, $K = 1$ and $x_f = 0.3$ (c) location of heater (x_f) and time lag (τ) with the other system parameters being $c_1 = 0.1$, $c_2 = 0.06$ and $K = 0.8$.

of machine tool vibrations by Kalmar-Nagy *et al.* [13] and Wahi & Chaterjee [22] for $\alpha = 3/4$. In the model for the heat release rate fluctuations in a Rijke tube, $\alpha = 1/2$, which implies that this model will exhibit subcritical Hopf bifurcation.

We had noted in our previous discussion in this section that the region where a stable steady state and a pair of stable and unstable limit cycles are seen to co-exist, is called the region of bistability. This is a general feature of systems exhibiting subcritical bifurcations and the region of bistability for the variation of non-dimensional heater power and the time lag is shown in Fig. 3.

4 Results & Discussions

4.1 On the effect of small time lag assumption

Traditionally delay differential equations governing the system dynamics in the thermoacoustic systems are linearized about $\tau = 0$ to get ordinary differential equations which are valid only for small time lags. The corresponding set of equations in the matrix form $d\chi/dt = L\chi$ is given in Balasubramanian & Sujith [3]. This matrix L can be used to calculate the eigenvalues of the system with small time lag assumption and the value of the parameters when the system becomes unstable can be noted as the stability boundary. This approximate stability boundary is compared with the exact stability boundary predicted by the system of delay differential equations given by Eqns. (7) and (8) in Fig. 4.

The linear stability boundaries showing the variation of the critical nondimensional heater power K, damping coefficient c_1 and the heater location x_f with the time lag in the system τ are shown in Figs. $4(a)$ to $4(c)$. It can be seen clearly that for all the three cases, the stability boundary predicted with the small time lag assumption does not match very well with the exact stability boundary of the delayed system. The curves approximately match when the time lag (τ) is very
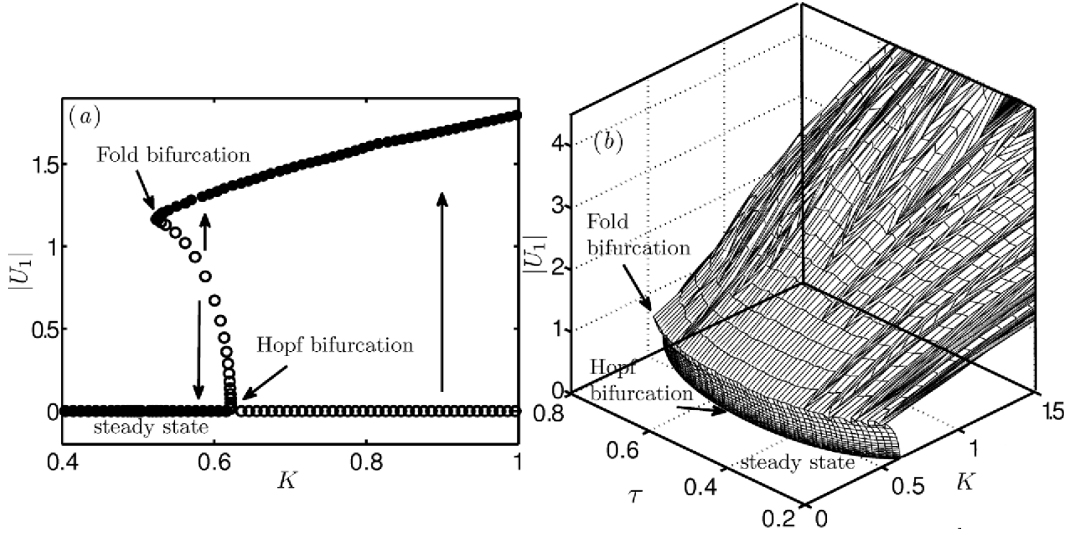
Figure 5: (a) Bifurcation plot for variation of non-dimensional heater power K. The other parameter values of the system are $c_1 = 0.1$, $c_2 = 0.06$, $x_f = 0.3$ and $\tau = 0.2$ (b) 3D plot of bifurcation plot of non-dimensional heater power K for varying values of time lag τ with the other parameters of the system $c_1 = 0.1$, $c_2 = 0.06$ and $x_f = 0.3$.

small. However, the match deteriorates very fast with an increase in the time lag (τ). Note from Fig. 4(b) that the small time lag assumption breaks down even at values of time lag such as $\tau = 0.1$ which are smaller than the typical values of time lag $\tau = 0.2$ [10,19]. In order to accurately predict the stability regions, linear stability boundary of thermoacoustic models with an explicit time-delay must therefore be calculated without invoking the small time lag assumption.

4.2 Effect of heater power

The effect of varying the non-dimensional heater power (K) on the evolution of the system is analyzed with the bifurcation diagram as shown in Fig. 5(a). Nondimensional heater power can be increased by increasing the current given to the electrical heater. For small values of K, the equilibrium is stable and all perturbations decay asymptotically resulting in steady flow within the tube. Increasing K decreases the margin of stability of the system and at a critical value of K, a pair of complex eigenvalues of the system cross over to the right half plane (Hopf bifurcation) and the system becomes linearly unstable resulting in an oscillating flow pattern in the tube.

The variation of $|U_1|$ with K is shown in Fig. 5(a). The empty circles indicate unstable solutions and filled circles indicate stable solutions. A limit cycle of very small amplitude is obtained first using the state at the Hopf point as the initial state and iterating using a Newton's scheme. As discussed earlier, the bifurcation is subcritical and the resulting small-amplitude limit cycles close to the Hopf point are unstable. These unstable limit cycles are obtained using numerical continuation of the limit cycle and they coexist with the stable equilibrium. This unstable branch of limit cycles further undergoes a fold or turning point bifurcation and gains stability.

The bifurcation diagram for the variation of the non-dimensional heater power is obtained for various values of time lag τ in the interval $[0.2, 0.8]$ and all the results are plotted along with the stability boundary for the system as a 3-D plot in $(\tau, K, |U_1|)$ in Fig. 5(b). From this 3-D bifurcation diagram, we can also obtain the 2-D bifurcation diagram involving the limit cycle amplitude variation with the time lag τ for a given value of K.
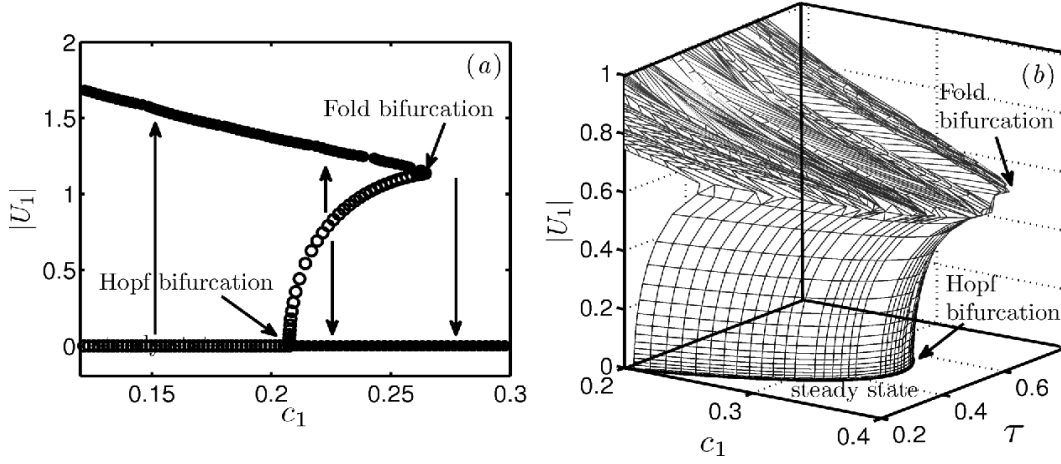
8

Figure 6: (a) Bifurcation plot for variation of damping coefficient c_1. The other parameter values of the system are $c_2 = 0.06$, $K = 1$, $x_f = 0.3$ and $\tau = 0.2$ (b) 3D plot of bifurcation plot of damping coefficient for varying values of time lag τ with the other parameters of the system $c_2 = 0.06$, $K = 1$ and $x_f = 0.3$.

4.3 Effect of damping

To study the effect of the variation of the amount of damping present in the system on the response of the system, one of the damping coefficients (c_1) of the mode dependent damping model is varied. Change in the damping of the system can be achieved in experiments by changing the end conditions of the duct. Increased damping has a stabilizing effect on the dynamics of the system and lowering of damping leads to instability. For lesser damping the equilibrium is either stable or unstable depending on the value of the time lag τ while for larger damping equilibrium is stable for any τ as shown in Fig. 4(b).

For a fixed time lag, there exists a critical value of c_1 below which all perturbations grow to limit cycles and above which there exists a region wherein large amplitude perturbations grow to limit cycles and small perturbations decay to the equilibrium as shown in Fig. 6(a). The critical value of the damping coefficient c_1 and the bifurcation diagrams has been obtained for various values of the time lag τ again and the results are plotted as a 3-D plot in Fig. 6(b). A 2-D projection of this plot on the (τ, c_1) plane gives us the linear stability boundary (Hopf points also shown in Fig. 4(b)) as well as the nonlinear stability boundary (fold points). The region enclosed between them gives us the bistable region to be discussed in more detail in subsequent subsections.

4.4 Effect of heater location

The location of the heat source (x_f) also has a very significant effect on the dynamics of the system and is achieved by placing the heater at different locations along the length of the duct. The stability of the system depends on the location of the heater along the duct in a non-monotonic manner. When the location of the heater along the duct is varied from the upstream open end, the system is initially linearly stable. At a critical value of the heater location x_{f1}, a pair of complex eigenvalues cross over to the right half plane and the system becomes linearly unstable. With further change in the location of the heater, the system remains linearly unstable till x_{f2}, when another Hopf bifurcation is observed in which a pair of complex eigenvalues cross from the right half plane to the left half plane and the system regains linear stability as also shown in Fig. 4(c).

The bifurcation plot for the variation of heater location (x_f) shows subcritical Hopf bifurcation at both the locations along the duct length corresponding to the Hopf bifurcation as shown in Fig. 7. The stable branch of limit cycles arising from the turning point bifurcations of the two branches of unstable limit cycles emanating from the Hopf points merge smoothly such that the region of
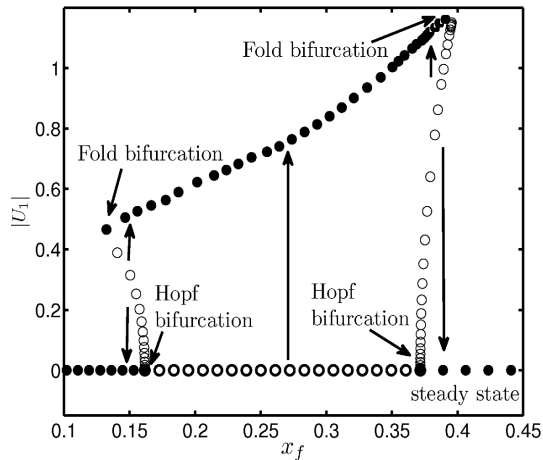
Priya Subrmanian, Sathesh Mariappan, R. I. Sujith & Pankaj Wahi

Figure 7: Bifurcation plot for variation of location of heater (x_f). The other parameter values of the system are $c_1 = 0.1$, $c_2 = 0.06$, $K = 0.8$ and $\tau = 0.2$.

linear instability is completely bounded by a single branch of nonlinearly stable limit cycles. Any initial condition within the linearly unstable region will asymptotically reach the corresponding stable limit cycle. The asymptotic state of an initial condition within the subcritical region is based on whether it is above or below the stable manifold of the unstable limit cycles. The amplitude of limit cycle is seen to be a strong function of the location of the heater and is seen to increase with an increase in the heater location from the open upstream condition.

4.5 Bistability regions

As discussed in section 3.2, there are regions of bistability for parameter ranges where the system can reach an equilibrium solution or a limit cycle depending on the initial conditions. This bistable region lies between the linear stability boundary given by the Hopf point and the nonlinear stability boundary given by the fold points. For the unstable region bounded by the Hopf bifurcation points, the system is unstable to any perturbation and hence, this region is termed as a globally unstable region. The system is globally stable to any perturbations for parameters in the region outside the nonlinear stability boundary (fold points) and this is called the region of global stability [20]. Thus the linear and nonlinear stability boundaries divide the parameter plane into three regions. The globally unstable region is shaded with light grey, the region filled with dark grey correspond to region of bistability and the white region represents globally stable region in Fig. 8.

Figure 8 shows the bistable regions along with the globally stable and unstable regions for variations of the damping coefficient (c_1) and the heater location (x_f) as functions of the time lag τ. The extremum value of the bistable regime typically appears at the parameter value τ at which the other parameter value corresponding to the linear stability boundary reaches an extremum itself.

5 Conclusions

The dynamical behavior of a model for a horizontal Rijke tube has been studied using the method of numerical continuation. Linear stability boundaries for the simultaneous variation of two parameters of the system are obtained. The stability predictions calculated by linearizing about the mean state with vanishing time lag are shown to be inaccurate. Therefore the calculation of linear stability boundary for systems modeled by time delay models, must be performed without the assumption of vanishingly small time lag in the system.

The nonlinear stability boundary and the regions of bistability where the system can reach one of the two possible asymptotic states are also obtained. Using the linear and nonlinear stability
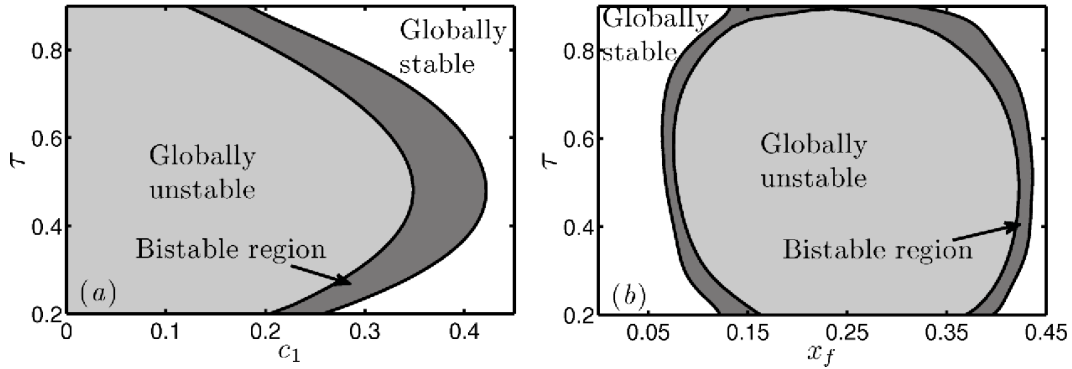
Figure 8: Region of bistability obtained for the bifurcation between (a) damping coefficient (c_1) and time lag (τ) with the other system parameters being $c_2 = 0.06$, $K = 1$ and $x_f = 0.3$ (b) heater location (x_f) and time lag (τ) with the other system parameters being $c_1 = 0.1$, $c_2 = 0.06$ and $K = 0.8$.

boundaries, regions of global stability, global instability and regions of potential instability are identified for the Rijke tube model. It has also been shown that only subcritical Hopf bifurcations are possible for the model considered to represent the behavior of the Rijke tube. Reduced order models of physical systems with explicit time delays can therefore be studied in detail using the method of numerical continuation to identify stability boundaries, to obtain bifurcation plots and to examine their possible dynamical behavior.

The authors wish to acknowledge Prof. M. K. Verma (IIT Kanpur) for discussions and Mr. Ashesh Saha (IIT Kanpur) for his guidance in using DDE-BIFTOOL.

References

[1] E. L. Allgower and K. Georg. *Numerical Continuation Methods: An Introduction.* Springer, 1990.

[2] N. Ananthakrishnan, S. Deo, and F. E. C. Culick. Reduced-order modeling and dynamics of nonlinear acoustic waves in a combustion chamber. *Combustion Science and Technology*, 177:221–248(28), 2005.

[3] K. Balasubramanian and R. I. Sujith. Thermoacoustic instability in a Rijke tube: Non-normality and nonlinearity. *Physics of Fluids*, 20:044103, 2008.

[4] J. A. Carvalho, M. A. Ferreira, C. Bressan, and L. G. Ferreira. Definition of heater location to drive maximum amplitude acoustic oscillations in a Rijke tube. *Combustion & Flame*, 76:17–27, 1989.

[5] Q. Ding, J.E. Cooper, and A.Y.T. Leung. Application of an improved cell mapping method to bilinear stiffness aeroelastic systems. *Journal of Fluids and Structures*, 20(1):35 − 49, 2005.

[6] K. Engelborghs, T. Luzyanina, and D. Roose. Numerical bifurcation analysis of delay differential equations using dde-biftool. *ACM Transactions on Mathematical Software*, 28(1):1–21, 2002.

[7] K. Engelborghs and D. Roose. Numerical computation of stability and detection of hopf bifurcations of steady state solutions of delay differential equations. *Advances in Computational Mathematics*, 10:271–289, 1999.

[8] C. A. Fannin, W. R. Saunders, M. A. Vaudrey, B. Eisenhower, and U. Vandsburger. Identification of a model for thermoacoustic instabilities in a Rijke tube. *IEEE Transactions on control systems technology*, 10:490–502, 2002.

[9] C. C. Hantschk and D. Vortmeyer. Numerical simulation of self-excited thermoacoustic instabilities in a Rijke tube. *Journal of Sound and Vibration*, 227:511–522, 1999.

[10] M. A. Heckl. Nonlinear acoustic effects in the Rijke tube. *Acustica*, 72:63–71, 1990.

[11] C. S. Hsu. A theory of cell-to-cell mapping dynamical systems. *Journal of Applied Mechanics*, 47(4):931–939, 1980.

[12] C. C. Jahnke and F. E. C. Culick. Application of dynamical systems theory to nonlinear combustion instabilities. *Journal of propulsion and power*, 10:508–517, 1994.

[13] T. Kalmar-Nagy, G. Stepan, and F. C. Moon. Subcritical hopf bifurcation in the delay equation model for machnie tool vibrations. *Nonlinear dynamics*, 26:121 – 142, 2001.

[14] Y. P. Kwon and B. H. Lee. Stability of the Rijke thermoacoustic oscillation. *Journal of the Acoustical Society of America*, 78:1414–1420, 1985.

[15] S. Mariappan and R. I. Sujith. Modeling nonlinear thermoacoustic instability in an electrically heated rijke tube. *48th AIAA Aerospace Sciences Meeting Including the New Horizons Forum and Aerospace Exposition, 4 - 7 January 2010, Orlando, Florida, AIAA 2010-25*, 2010.

[16] K. I. Matveev. *Thermo-acoustic instabilities in the Rijke tube: Experiments and modeling*. PhD thesis, California Institute of Technology, Pasadena, 2003.

[17] K. Mcmanus, T. Poinsot, and S. Candel. A review of active control of combustion instabilities. *Progress in Energy and Combustion Science*, 19:1 – 29, 1993.

[18] J. P. Moeck, M. R. Bothien, S. Schimek, A. Lacarelle, and C. O. Paschereit. Subcritical thermoacoustic instabilites in a premixed combustor. *14th AIAA/CEAS Aeroacoustics Conference*, page 2946, 2008.

[19] F. Selimefendigil, R. I. Sujith, and W. Polifke. Identification of heat transfer dynamics for non-modal stability analysis of thermoacoustic systems. *AIP Conference Proceedings*, 1168(1):605–608, 2009.

[20] S. H. Strogatz. *Nonlinear Dynamics and Chaos: with applications to Physics, Biology, Chemistry, and Engineering*. Westview Press, Colorado, first edition, 2000.

[21] H. Tamura, A. Sueoka, and Y. Tsuda. higher approximation of steady oscillations in nonlinear systems with single degree of freedom suggested multi-harmonic balance method. *Journal of the Society of Mechanical Engineers-Bulletin*, 24:1616 – 1625, 1981.

[22] P. Wahi and A. Chatterjee. Regenerative tool chatter near a codimension 2 hopf point using multiple scales. *Nonlinear Dynamics*, 40:323–338, 2005.

[23] J. M. Wicker, W. D. Greene, S. I. Kim, and V. Yang. Triggering of longitudinal combustion instabilities in rocket motors: nonlinear combustion response. *Journal of Propulsion & Power*, 12:1148–1158, 1996.

[24] B. T. Zinn and M. E. Lores. Application of the Galerkin method in the solution of non-linear axial combustion instability problems in liquid rockets. *Combustion Science & Technology*, 4:269–278, 1971.